Fuzzy Pulmonary Vessel Segmentation Using Optimized Vessel Enhancement Filtering

Jens N. Kaftan[1,2], Atilla P. Kiraly[3], Marius Erdt[4],
Michael Sühling[2], and Til Aach[1]

[1] Institute of Imaging and Computer Vision, RWTH Aachen University,
52056 Aachen, Germany,
jens.kaftan@lfb.rwth-aachen.de
[2] Siemens Healthcare Sector, Computed Tomography, 91301 Forchheim, Germany
[3] Siemens Corporate Research, Princeton, NJ 08540, USA
[4] Fraunhofer Institute for Computer Graphics, Cognitive Computing &
Medical Imaging, 64283 Darmstadt, Germany

Abstract. Vessel segmentation within pulmonary images serves as a basis for a variety of applications, including PE detection and visualization, lung nodule detection, assistance in bronchoscopic navigation, lobe segmentation, and surgical planning. Although applications have different segmentation requirements, speed and accuracy is a clear benefit. A new approach combining a single parameter vessel enhancement filter and fuzzy connectedness is presented. The advantages of vessel filtering are brought to bear with a minimal impact on time by limiting the scales. Vesselness and intensity features are combined within a fuzzy segmentation framework, reducing the number of required scales and avoiding some of the drawbacks of each feature alone. Validation was performed on five datasets and Dice Similarity Coefficients (DSC) demonstrate an improvement of 9% (from 81% to 90%) on average for small vessels without influencing the accuracy for large vessels (95%) compared to an intensity-based method alone.

1 Introduction

Vascular tree segmentation in pulmonary computed tomography (CT) images is a core component of a variety of applications. Both the computer-aided diagnosis (CAD) and visualization of pulmonary emboli (PE) require vessel segmentation [1–3]. Although smaller vessels may have less direct clinical relevance, segmentation of these vessels can provide important information for tree hierarchy, lobar lung segmentation, and lung region assessment [4]. In PE CAD, the segmentation is used to reduce false positives while in visualization the segmentation is used as a basis for display. The same holds true for lung nodule CAD [5]. Navigation through the airways can make use of the vessel segmentation as well [6]. Finally, scoring and determining bronchio-arterial ratios within the airways also makes use of vessel segmentation [7].

Several challenges face vessel segmentation methods. Variations in attenuation due to partial volumes effects and the presence of PE can limit the segmentation extent. Nearby high density structures such as airway walls or connective

tissue can be confused with vessels. Finally, arteries and veins in close proximity can cause their segmentations to overlap [4, 8]. Although we do not address this last issue, we believe that an improved segmentation is also advantageous for artery-vein separation methods.

Intensity-based segmentation approaches using either threshold-based methods [4, 9, 10], front propagation techniques [8], or fuzzy techniques [11] have proven to be very efficient. These methods use an intensity model that is directly or indirectly utilized to detect and delineate vessels. However, due to variations in intensity as explained above, these methods tend to leak into surrounding non-vessel structures in some areas while missing smaller vessels.

Vessel enhancement filters, such as the Hessian-based filters [12, 13] have proven to be very capable in vessel segmentation. These methods compute eigenvalues of the Hessian matrix and combine them into a final value. These filters need to be applied at multiple scales to capture vessels of varying diameters. Approaches such as Zhou et al. [1] use up to 12 different scales. Speed quickly becomes an issue when multiple scales are used. Additionally, bifurcations usually do not have high responses to line-filters resulting in disconnected pieces.

We propose to use vessel enhancement filtering (Section 2) in combination with our intensity-based fuzzy approach [11]. Compared to other enhancement techniques our filter response function has been analytically designed to combine the eigenvalues of the Hessian matrix in such a way, that the output becomes maximal for tubular structures with Gaussian intensity profile. In particular it does not rely on any other parameter than the scale factor [14]. We demonstrate that this combination (Section 3) allows for accurate vessel segmentation with only a few filter scales, which would not be possible with vesselness filters alone. In addition, the intensity information is capable of steering the fuzzy-connectedness region growing process in areas such as bifurcations for which the filter output is lacking. The result is a synergy of the benefits of the individual methods compensating their individual drawbacks. The speed of intensity-based methods is preserved with the specificity benefits of vessel filtering (Section 5).

2 Optimized Vessel Enhancement

Vessel enhancement filters are typically based on the eigenvalues of the Hessian matrix H [12, 13] and have already been successfully applied to pulmonary vessel segmentation [1, 15]. In practice, the image signal is convolved with the six second order derivatives of the Gaussian g and the eigenvalues of the resulting Hessian matrix are combined into a filter output that enhances tubular-like structures.

Assuming that a vessel $v(\mathbf{r})(\mathbf{r} = (x, y, z))$ can be modeled locally by a cylinder with a radial Gaussian intensity profile with, e.g., a, b being the intensity values at the vessel center and boundary, respectively, which is orientated along the x-axis for the following considerations,

$$v(\mathbf{r}) = b + (a - b) \exp - \frac{y^2 + z^2}{2\sigma_v^2} \tag{1}$$

we compose the filter $h(\mathbf{r})$ as a linear combination of second order derivatives of the Gaussian with the standard deviation σ_h chosen to be the same as the standard deviation of the vessel model σ_v such that its convolution with this ideal vessel signal $v(\mathbf{r})$ is maximized [14]

$$S = v * h = \int_{\mathbb{R}^3} v(\mathbf{r}) h(-\mathbf{r}) d\mathbf{r} \tag{2}$$

This can be solved analytically using the mathematical framework of Lagrange multipliers yielding

$$h(\mathbf{r}) = c \cdot \left(\frac{2}{3} g_{xx}(\mathbf{r}) - g_{yy}(\mathbf{r}) - g_{zz}(\mathbf{r}) \right) \tag{3}$$

with $c = \sqrt{\frac{3}{5\pi^{3/2}}} \cdot \sqrt{\sigma_v}$.

In reality, the orientation of the vessel is not known, but the filter has to be oriented along the vessel to obtain maximum response. This direction is equal to the eigenvector corresponding to the eigenvalue with the smallest magnitude of the Hessian matrix. Let the eigenvalues of H be $\lambda_{1,2,3}$ with $|\lambda_1| \leq |\lambda_2| \leq |\lambda_3|$, then the optimal filter output can be computed as:

$$S_{\text{opt}} = v * h_{\text{rot}} = \frac{2}{3}\lambda_1 - \lambda_2 - \lambda_3 \tag{4}$$

Since vessel structures are brighter than the background we expect $\lambda_{2,3} < 0$. Unfortunately, very bright, plate-like structures for which the cross-sectional profile is Gaussian only in one direction, i.e., the intensity decreases rapidly in one direction but not in the orthogonal one, the filter output might still become large because of either $|\lambda_2|$ or $|\lambda_3|$ being large. Hence, we multiply the filter output (4) by an isotropy factor

$$\kappa = \begin{cases} 0 & \text{if } \lambda_2 > 0 \text{ or } \lambda_3 > 0 \\ 1 - \frac{|\lambda_2| - |\lambda_3|}{|\lambda_2| + |\lambda_3|} & \text{else} \end{cases} \tag{5}$$

As the pulmonary vascular structure consists of vessels with varying diameters, multiscale results are therefore obtained combining the filter output at different scales σ_{h_i}. It can be shown that the filter output with an idealized vessel is proportional to $\sigma_h^{3/2}$, which needs to be accounted for

$$S_{\text{opt}} = \max \left(\kappa \cdot \sigma_{h_i}^{-3/2} \cdot S_{\text{opt}}(\sigma_{h_i}) \right) \ \forall \ i \tag{6}$$

Results of the optimized vesselness filter, shown in Figure 1, allow for a clear distinction between vessel- and non vessel-like structures. Fig. 1a shows the original HU values while in Fig. 1b the lung regions have been replaced by the filter output. Additionally we have recently shown its applicability to liver vessel enhancement in CT data [14]. Note that compared to other Hessian-based techniques such as [12], our filter function requires only a single parameter (scale).

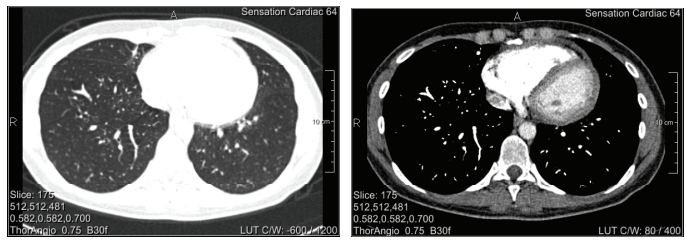

(a) Original (b) Filter output

Fig. 1. Contrasted CT dataset of the lung. (a) Original (lung window) and (b) visualization for which the lung areas have been replaced by the filter output using $\sigma_h = [1, 2, 4]$ mm while the body regions are shown as original value (vessel window).

3 Combined Fuzzy Segmentation

For the sake of completeness we will first briefly review our general fuzzy segmentation framework [11] before detailing the incorporation of the vesselness filter output into the intensity-based system and discussing the different parameters.

3.1 Fuzzy Vessel Segmentation

Assuming a segmentation of the left and right lung [16] is already given, we first detect multiple seed points throughout the whole lung. To this end we segment the major vessels with a high specificity using an intensity-based method [4]. Hence we apply a lower threshold $T = 150$ HU and eliminate components smaller than $V_{min} = 500$ voxels in size. Next each resulting component is converted into one or more seed-points by locating and clustering vessel points with locally maximal distance to the vessel surface utilizing a 3D distance transformation. The cluster representatives $\mathbf{s}_i$ are selected with preference to large distance values, i.e., large radius estimates. Assigning to the so detected seed-points a probability measure of $P_{\text{vessel}}(\mathbf{s}_i) = 1$, we calculate the probability measure for the remaining voxels using the fuzzy connectedness algorithm [17].

The likelihood that two neighboring voxels $\mathbf{c}, \mathbf{d}$ belong to the same class, here to the vascular tree, is described by the local affinity $\mu_\kappa(\mathbf{c}, \mathbf{d})$. Using, e.g., an intensity-based probability function, the affinity can be defined as

$$\mu_\kappa(\mathbf{c}, \mathbf{d}) = \begin{cases} e^{-\frac{1}{2\sigma^2}\left(\frac{f(\mathbf{c})+f(\mathbf{d})}{2}-\mu\right)^2} & \text{if } \frac{f(\mathbf{c})+f(\mathbf{d})}{2} < \mu \\ 1 & \text{else} \end{cases} \tag{7}$$

with $f(\mathbf{c})$ being the intensity value at position $\mathbf{c}$ and μ, σ^2 being the expected intensity value and variance of the used Gaussian function. The "strength of connectedness" μ_N of two distant voxels $\mathbf{c}, \mathbf{d}$ along a certain path $p_{\mathbf{c},\mathbf{d}}$ is simply

the smallest pairwise fuzzy affinity along this path. A path $p_{\mathbf{c},\mathbf{d}}$ from $\mathbf{c}$ to $\mathbf{d}$ is a sequence of $m > 2$ neighboring voxels $\langle \mathbf{c}^{(1)} = \mathbf{c}, \mathbf{c}^{(2)}, ..., \mathbf{c}^{(m)} = \mathbf{d} \rangle$, i.e.,

$$\mu_N(p_{\mathbf{c},\mathbf{d}}) = \min \left[\mu_\kappa(\mathbf{c}^{(1)}, \mathbf{c}^{(2)}), ..., \mu_\kappa(\mathbf{c}^{(m-1)}, \mathbf{c}^{(m)}) \right] \tag{8}$$

The global connectivity $\mu_K(\mathbf{c}, \mathbf{d})$ is then the largest of the strength of connectedness of all possible paths $\mathbb{P}_{\mathbf{c},\mathbf{d}}$ between $\mathbf{c}, \mathbf{d}$:

$$\mu_K(\mathbf{c}, \mathbf{d}) = \max_{p_j \in \mathbb{P}_{\mathbf{c},\mathbf{d}}} [\mu_N(p_j)] \quad \forall\, j \tag{9}$$

The probability measure that a voxel $\mathbf{x}$ belongs to a vessel is hence:

$$P_{\text{vessel}}(\mathbf{x}) = \max_{\mathbf{s}_i} [\mu_K(\mathbf{x}, \mathbf{s}_i)] \quad \text{with} \quad P_{\text{vessel}}(\mathbf{s}_i) = 1 \ \ \forall\, i \tag{10}$$

Note that even if P_{vessel} drops below 0.5 for a voxel, this voxel can still most likely belong to the vascular tree. In fact, an appropriate threshold has to be applied for binarization.

3.2 Feature Combination

Using an intensity-based function alone, one can observe that small vessels that are significantly darker than large vessels are often missed while already leaking into non-vessel structures. Hence it is reasonable to focus on small vessels when applying the vessel enhancement filter while vessels of larger scale are segmented well using an intensity-based function alone. Additionally to minimize the computational complexity we prefer to use as few filter scales as possible. A combination of $\sigma_h = [1, 2, 4]$ mm have been experimentally determined to be a good choice (see also Fig. 1). Having now the original and filter output values, the local affinity becomes a multimodal function with $\mu_{\kappa_{\{1,2\}}}(\mathbf{c}, \mathbf{d})$ being dependent on the parameters $\mu_{\{1,2\}}, \sigma^2_{\{1,2\}}$ and $f_{\{1,2\}}(\mathbf{c})$ being the intensity value and filter output at $\mathbf{c}$, respectively. The scalar output of μ_κ has been chosen to be the maximum value of $\mu_{\kappa_{\{1,2\}}}$. The parameters $\mu_{\{1,2\}}$ are the average intensity and filter output values of the seed points $\mathbf{s}_i$ while $\sigma^2_{\{1,2\}}$ have to be chosen (Sec. 5).

Consequently, the fuzzy connectedness region growing targets large vessels via the intensity-based function and smaller vessels via the filter output. However, in areas where the filter output is locally low, such as it is the case for some bifurcations, the intensity-based function will still prevent the growing process to terminate early. That is, locally low filter responses will not cause additional vessels to be missed while also having no impact on the false positive rate.

4 Validation

The validation of pulmonary vessel segmentation systems is especially difficult because of the complexity and size of the vascular tree structure. Often such methods are only qualitatively validated because of a missing ground truth

for clinical data. Additionally some authors estimate the accuracy of their approaches by counting the number of manually placed centerline points that are included into the segmentation output [1], which however allows no quantification of false positive regions. Wu et al. [9] compare their segmentation results of clinical data with additive artificial noise to the result of the original data. Such evaluation feature indicates the robustness of the segmentation method against noise but does not quantify the segmentation accuracy itself.

We use a fast, semi-automatic method to create reference segmentation in sub-volumes based on the random walker algorithm [18, 19]. The user first defines a 3D region of interest (ROI) and threshold-based fore- and background seed points are added within this subvolume. These seeds are then used as initialization for the random walker algorithm, a graph-based segmentation approach that can be used for interactive segmentation purposes. To this end, each voxel is represented by a node and neighboring voxels are connected by weighted edges using a weighting function, such as

$$w_{ij} = \exp\left(-\beta \cdot \Delta d_{ij} \cdot |I(\mathbf{x}_i) - I(\mathbf{x}_j)|\right) \tag{11}$$

Here $I(\mathbf{x}_i)$ is the intensity value of voxel i, Δd_{ij} the distance between voxel i and j and β a free parameter (here: $\beta = 150$). Next, the random walker algorithm is consecutively applied along with user interaction until the segmentation output is sufficiently accurate. Although strictly spoken one would have to validate the semi-automatically created segmentation results itself, which is as already discussed difficult due to a missing ground truth, the characteristics of the described method indicates that it is very well suited for validation purposes:

- The random walker algorithm allows the creation of any arbitrary segmentation given enough seed points, i.e., the user is not bounded by the system [18].
- Only a comparibly small number of seed points is required to produce a segmentation that is almost identical to a manual segmentation [19].
- Variations of the exact position of the seed points results only in small differences in the final result, i.e., the method allows the creation of results with a higher reproducability than manual methods [19].

Using the so created reference segmentations for quantitative validation and parameter optimization we use sensitivity ($\frac{TP}{TP+FN}$), specificity ($\frac{TN}{TN+FP}$), and the Dice similarity coefficient (DSC)

$$DSC = \frac{2 \cdot TP}{2 \cdot TP + FP + FN} \tag{12}$$

with TP, FP, and FN being the true positive, false positive, and false negative voxel count as validation features. Note that each threshold for P_{vessel} will result in one set of features.

Although the semi-automatically created reference segmentations have a high accuracy, they are still limited by the time the radiologist (or any other medical expert) can spend on their creation. We avoid superficial differences between the automatic segmentation and the ground truth from influencing the results

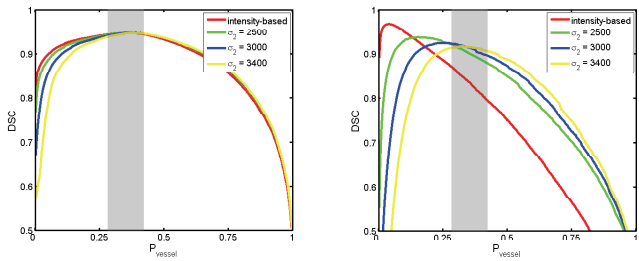

(a) DSC for large vessels (b) DSC for small vessels

Fig. 2. DSC for all datasets with varying parameters. The red curves show the performance using the intensity-based method only. For larger vessels (a) the variation of parameters does not have any significant influence on the accuracy within the optimal band of thresholds highlighted by the gray bar. In (b) one can see that the inclusion of the vesselness criteria shifts the DSC curve for small vessels towards higher thresholds.

by not counting voxels within a margin of one voxel along the outer vessel surface as neither positive nor negative. This methodology also reduces a potential validation bias since the interior segmentation should be more independent on the semi-automatic method than the contour.

5 Results

The proposed method has been evaluated on five different randomly selected contrast enhanced chest CT scans from clinical routine of patients referred for PE. These data have been acquired using Siemens Sensation 16/64 scanners with voxel sizes ranging from 0.55-0.7 mm in x, y and 0.6-0.7 mm in z-direction. For quantitative validation 30 manually selected ROIs of size 50^3 voxel have been semi-automatically segmented. For each patient, two ROIs have been randomly placed in regions of large vessels and four in regions of small vessels within the periphery of the lung. Although the intensity-based method alone provides in general good results, the evaluation of large and small vessels individually (Fig. 2, red curves) reveals that for thresholds of the probability measure P_{vessel} that are very well suited for large vessels, the accuracy for small vessels is not optimal.

Adding the output of the vesselness filter to the fuzzy segmentation method does especially increase the segmentation accuracy of smaller vessels for high and medium thresholds without significantly affecting, as expected, the segmentation output for large vessels, since we apply the filter for smaller scales only. The comparison for different parameter settings of σ_1 and σ_2 are shown in Figure 2. In fact, only the ratio between both parameters is of importance when combining both affinity features, hence we keep $\sigma_1 = 200$ HU constant while varying $\sigma_2 \in [2500, 3400]$. One can observe that an increased value of σ_2 will shift the DSC

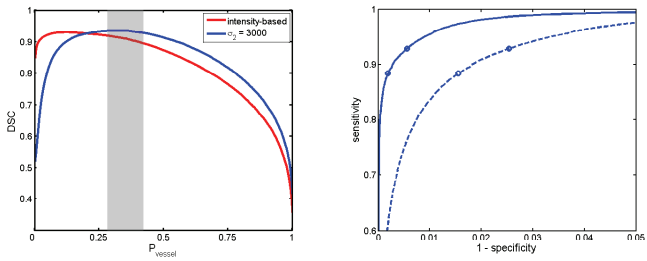

(a) DSC incl. large and small vessels (b) ROC incl. large and small vessels

Fig. 3. Dice similarity coefficient and ROC curve for all datasets including large and small vessels with varying parameters. (a) The red curve shows the DSC using the intensity-based method only and the blue curve using a combination with $\sigma_2 = 3000$. Note that the blue curve has its optimum in the middle of the preferred threshold range. (b) ROC curves with (solid line) and without the one voxel security margin (dashed line) used for evaluation. The circles represent the operating points of the left and right boundary of the band of optimal thresholds, respectively.

curve for small vessels towards higher threshold. Unfortunately, the maximum accuracy also decreases slightly with increasing σ_2. This is most likely caused by introducing also some false positive regions by the vesselness feature, where the filter output responses relatively high to non-vessel structures. Note, however, that the optimal threshold for small vessels using the intensity feature alone has practically no relevance since it would cause severe leakage in other regions. Taking this into account a parameter of $\sigma_2 = 3000$ (blue curve) turns out to be a good compromise as its DSC just turns to its maximal value at the left boundary of the specified optimal range of thresholds. Using, e.g., a threshold for P_{vessel} of 0.4 that segments the vessels relevant for PE applications consistently well, the DSC increases from 81% to 90% for small vessels while being 95% for large vessels. Comparing the intensity-based function only with the combination using $\sigma_2 = 3000$, the overall DSC curves are shown in Figure 3a. The overall sensitivity and specificity within the band of optimal thresholds varies between $88.4-92.9\%$ and $99.8-99.4\%$ with security margin and between $88.4-92.9\%$ and $98.4-97.5\%$ without the security margin (Fig 3b).

Segmentation examples are shown in Figure 4 using a threshold for P_{vessel} of 0.4. The top row shows that the proposed method (right) is able to capture more vessels than the purely intensity-based method (left). For the example shown in the lower row even a reduction of the threshold for P_{vessel} to 0.2 for the intensity-based method would only cause severe leakage into non-vessel structures but not the inclusion of the missed vessel. The vessel segmentation without vesselness filters typically requires 30 seconds. The addition of the filter responses adds about 20 seconds (per scale) to this time on a common PC. However, more efficient implementations involving the GPU reduce this time drastically [14].

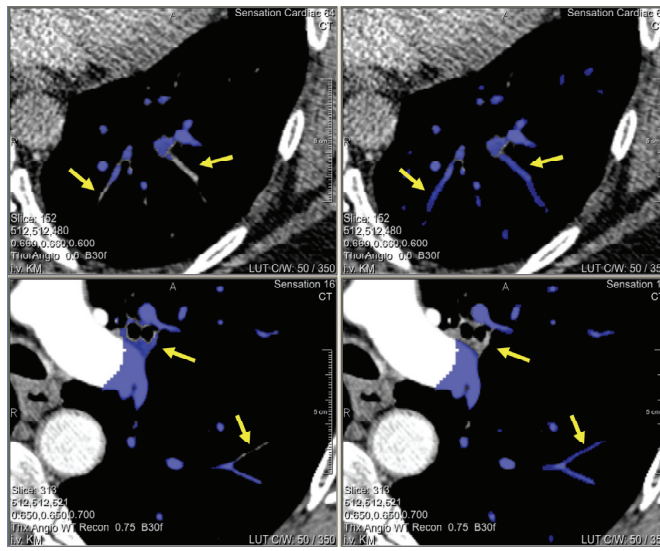

Fig. 4. Segmentation result using the proposed method (right) in comparison to the intensity-based method (left) for two different patients (best viewed in color). One can observe that the new segmentation extends further to the periphery than the purely intensity-based one.

6 Summary and Conclusions

We have presented a vessel segmentation method combining a minimal parameter vesselness filter with fuzzy connectedness. The method combines the filter output with an intensity model in our fully automatic fuzzy approach to pulmonary vessel segmentation in contrast enhanced CT data. One can observe that using intensity features alone the optimal thresholds band suited for large vessels does not overlap with the band for small vessels. Hence such methods tend to leak into surrounding non-vessel structures in close proximity to larger vessels while missing smaller vessels. The results show that using the combination improves the DSC by 9% (from 81% to 90%) for small vessels without influencing the accuracy for large vessels (95%) compared to the intensity-based method alone. Additionally we were able to limit the number of required vesselness filter scales to three, resulting in a computationally efficient method. The result is a method with the benefits of the vesselness filter, i.e., accuracy, and the intensity model, i.e., speed, without the drawback of each method individually. In the future we plan to extend the validation to more datasets, especially also to patients with other lung deseases.

References

1. Zhou, C., Chan, H.P., et al.: Automatic multiscale enhancement and segmentation of pulmonary vessels in CT pulmonary angiography images for CAD applications. Med. Phys. **34**(12) (2007) 4567–4577
2. Kiraly, A.P., Novak, C.L., et al.: A comparison of 2D and 3D evaluation methods for pulmonary embolism detection in CT images. In: SPIE MI. Vol. 6146. (2006) 132–140
3. Masutani, Y., MacMahon, H., Doi, K.: Computerized detection of pulmonary embolism in spiral ct angiography based on volumetric image analysis. IEEE TMI **21**(12) (2002) 1517–1523
4. Kiraly, A.P., Pichon, E., et al.: Analysis of arterial subtrees affected by pulmonary emboli. In: SPIE MI. Vol. 5370. (2004) 1720–1729
5. Agam, G., Armato III, S.G., Wu, C.: Vessel tree reconstruction in thoracic CT scans with application to nodule detection. IEEE TMI **24**(4) (2005) 486–499
6. Geiger, B., Kiraly, A.P., et al.: Virtual bronchoscopy of peripheral nodules using arteries as surrogate pathways. In: SPIE MI. Vol. 5746. (2005) 352–360
7. Kiraly, A.P., Odry, B.L., et al.: Computer-aided diagnosis of the airways: Beyond nodule detection. Journal of Thoracic Imaging **23**(2) (2008) 105–113
8. Buelow, T., Wiemker, R., et al.: Automatic extraction of the pulmonary artery tree from multi-slice CT data. In: SPIE MI. Vol. 5746. (2005) 730–740
9. Wu, C., Agam, G., et al.: Regulated morphology approach to fuzzy shape analysis with application to blood vessel extraction in thoracic CT scans. In: SPIE MI. Vol. 5370. (2004) 1262–1270
10. Masutani, Y., MacMahon, H., Doi, K.: Automated segmentation and visualization of the pulmonary vascular tree in spiral CT angiography: An anatomy-oriented approach based on three-dimensional image analysis. Journal of Computer Assisted Tomography **25**(4) (2001) 587–597
11. Kaftan, J.N., Kiraly, A.P., et al.: Fuzzy pulmonary vessel segmentation in contrast enhanced CT data. In: SPIE MI. Vol. 6914, 69141Q. (2008)
12. Frangi, A.F., Niessen, W.J., et al.: Multiscale vessel enhancement filtering. Lecture Notes in Computer Science **1496** (1998) 130–137
13. Sato, Y., Nakajima, S., et al.: Three-dimensional multi-scale line filter for segmentation and visualization of curvilinear structures in medical images. Medical Image Analysis **2**(2) (1998) 143–168
14. Erdt, M., Raspe, M., Sühling, M.: Automatic hepatic vessel segmentation using graphics hardware. In: 4th Int Workshop on Medical Imaging and Augmented Reality (MIAR). (2008) to appear.
15. Shikata, H., Hoffman, E.A., Sonka, M.: Automated segmentation of pulmonary vascular tree from 3D CT images. In: SPIE MI. Vol. 5369. (2004) 107–116
16. Hu, S., Hoffman, E.A., Reinhardt, J.M.: Automatic lung segmentation for accurate quantitation of volumetric x-ray ct images. IEEE TMI **20**(6) (2001) 490–498
17. Udupa, J.K., Samarasekera, S.: Fuzzy connectedness and object definition: theory, algorithms, and applications in image segmentation. Graph. Models Image Process. **58**(3) (1996) 246–261
18. Grady, L.: Random walks for image segmentation. IEEE Trans on PAMI **28**(11) (2006) 1768–1783
19. Grady, L., Schiwietz, T., et al.: Random walks for interactive organ segmentation in two and three dimensions: Implementation and validation. In: Proc of MICCAI. LNCS 3750 (2005) 773–780